Electronic Supplementary Material (ESI) for Inorganic Chemistry Frontiers.

Eu^{3+}-MOF fluorescence sensor based on dual-ligand strategy for visualization assay of an anthrax biomarker 2,6-pyridine dicarboxylic acid

Runnan Wang[a,b], Hao Zhang[b], Jing Sun[*,a], Zhongmin Su[*,a]

[a] *School of Chemistry and Environmental Engineering, Changchun University of Science and Technology, Jilin Provincial Science and Technology Innovation Center of Optical Materials and Chemistry, Jilin Provincial International Joint Research Center of Photo functional Materials and Chemistry, Changchun, 130022, People's Republic of China.*

[b]*Department of Analytical Chemistry, Jilin Institute of chemical Technology, the Key Laboratory of Fine Chemicals of Jilin Province, Jilin, 132022, PR China.*

*correspondence: sj-cust@126.com; zmsu@nenu.edu.cn

Reagents: $Eu(NO)_3 \cdot 6H_2O$, 2,5-thiophenedicarboxylic acid (H_2TDA), 2-aminoterephthalic acid (NH_2-BDC), 2,6-pyridine dicarboxylic acid and N,N-Dimethylformamide (DMF), ethyl alcohol (EtOH), methyl alcohol (MeOH), acetonitrile (ACN), isopropanol (IPA), benzene (PhH), methylbenzene (PhMe), dichlorotoluene (2,4-DCT), N,N-Dimethylaniline (DMA), ethyl acetate (EA) and 1-Pentanol (PEN), Benzoic acid, p-phthalic acid, Iso-phthalic Acid, Isonicotinic acid were purchased from Aladdin BioChem Technology Co. Ltd. Fetal calf serum and amino acid including Gly, Arg, Lys, Asp and Met were purchased from Shanghai Macklin Biochemical Technology Co., Ltd. All the chemicals were commercially purchased and used without further purification.

Methods: The powder X-ray diffraction (PXRD) measurements were carried out on a D8 Advance diffractometer with Cu kα radiation and recorded in the 2θ range of 5-60° and the simulated powder patterns of Eu-MOF were calculated using Mercury 3.8 via CIF files. The single crystal X-ray was measured on a Bruker APEX-II CCD diffractometer with graphite monochromatic Mo Ka radiation at 298 K. A Thermo Fisher Scientific thermogravimetric analyzer apparatus was implemented for TGA curves with a heating rate of 5 °C/min from room temperature to 800 °C/min under a N_2 atmosphere to determine. Fourier transform infrared (FT-IR) spectroscopy performed by a Thermo Fisher Scientific Nicolet iS 50 spectrometer in the range of 4000-400 cm^{-1} with a powder sample on a KBr pellets. X-ray photoelectron spectra (XPS) was collected on a Thermo Fisher Scientific ESCALAB 250XI device. All the fluorescence spectrum analysises were recorded on a HORIBA Fluoromax TCSPC fluorescence spectrometer. The SEM images were observed on a JEOL JSM-7610F Plus.

Crystallography: Structures were solved by direct methods and refined by a full matrix least-squares technique based on F^2 embedded in SHELXTL program through using the Olex2 as the graphical interface. All hydrogen atoms were placed geometrically in ideal positions with a riding model, and all non-hydrogen atoms were refined by the anisotropic thermal parameters during the final cycles.

Computational methods:

Intermolecular forces: The density functional theory (DFT) calculations were carried out with the VASP code[1]. The Perdew-Burke-Ernzerhof (PBE) functional within generalized gradient approximation (GGA)[2] was used to process the exchange-correlation, while the projectoraugmented-wave pseudopotential (PAW)[3] was applied with a kinetic energy cut-off of 500 eV, which was utilized to describe the expansion of the electronic eigenfunctions. The vacuum thickness was set to be 25 Å to minimize interlayer interactions. The Brillouin-zone integration was sampled by a Γ-centered 5×5×5 Monkhorst-Pack k-point. All atomic positions were fully relaxed until energy and force reached a tolerance of 1×10^{-5} eV and 0.03 eV/Å, respectively. The dispersion corrected DFT-D method was employed to consider the long-range interactions[4].

HOMO and LUMO energies: The initial molecular structure selected was constructed using GaussView6.0 software using DFT functional B3LYP-D3, 6-31G(d) basis set for C, H, O, N, S and dispersion-corrected for hydrogen bonding. The calculations are performed on the Gaussian 16 program.

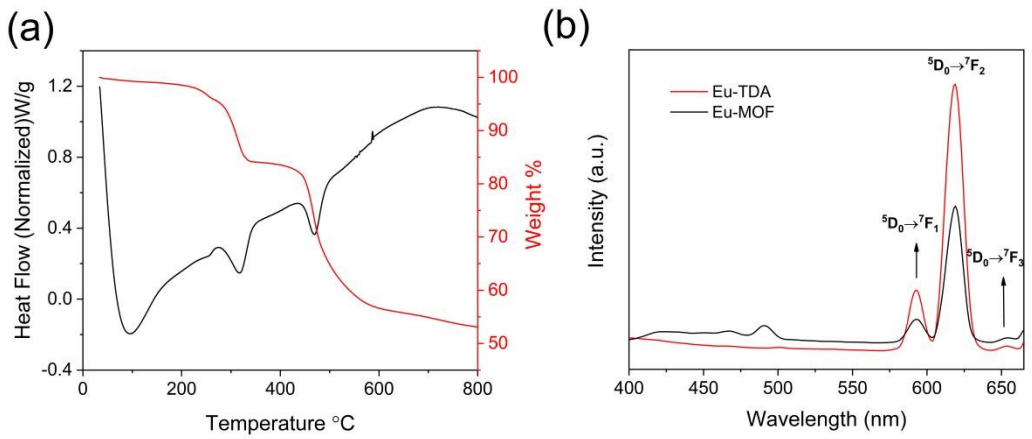

Fig. S1. (a) Thermogravimetric analysis of Eu-MOF (b) The solid-state luminescence spectra of Eu-MOF and Eu-TDA.

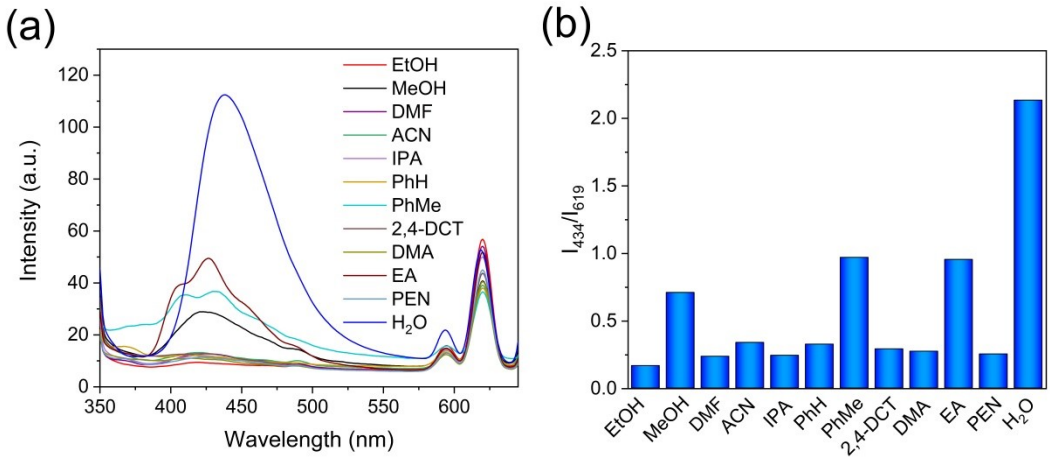

Fig. S2. (a) Luminescence intensity of Eu-MOF dispersed in different solvents. (b) The fluorescence intensity ratio of I_{434}/I_{621}.

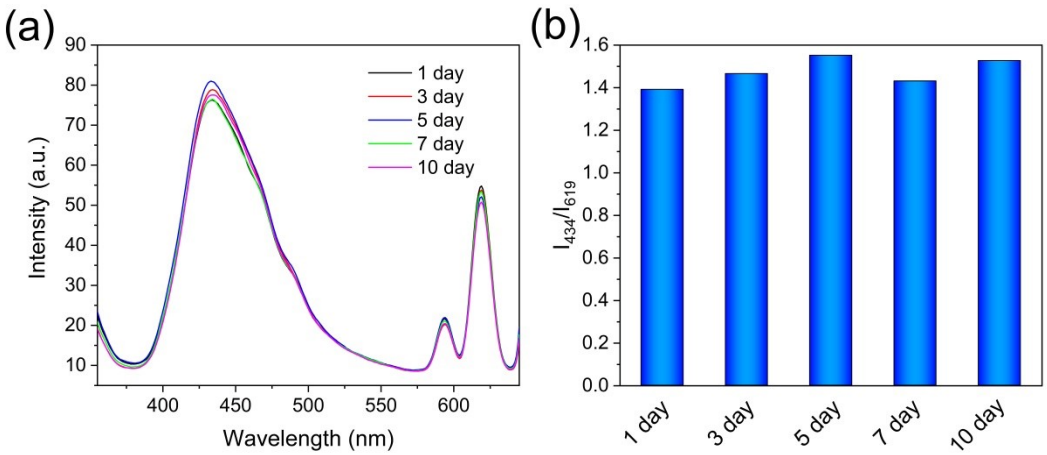

Fig. S3. (a) Luminescence intensity of Eu-MOF soaked in ethanol-water (V:V=9:1) solution for different days. (b) The fluorescence intensity ratio of I_{434}/I_{621}.

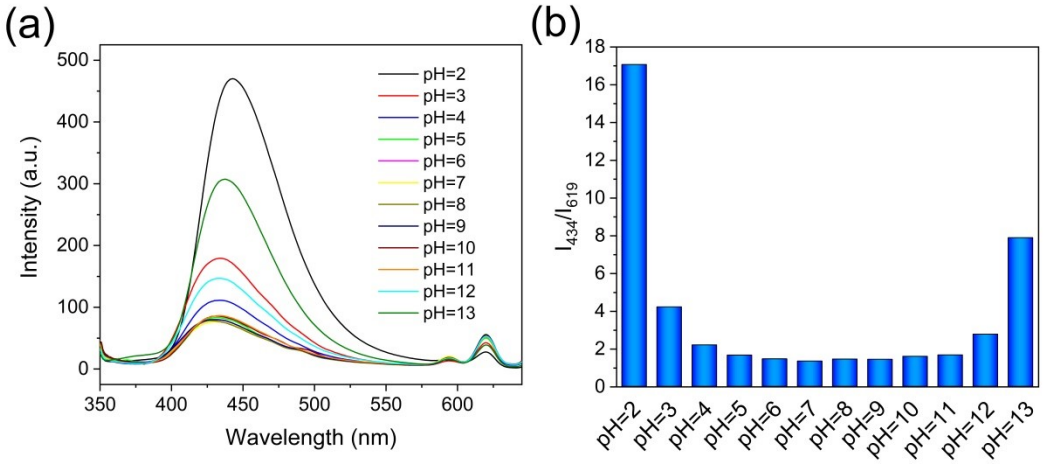

Fig. S4. (a) Luminescence intensity of Eu-MOF in different pH of ethanol-water (V:V=9:1) solution. (b) The fluorescence intensity ratio of I_{434}/I_{621}.

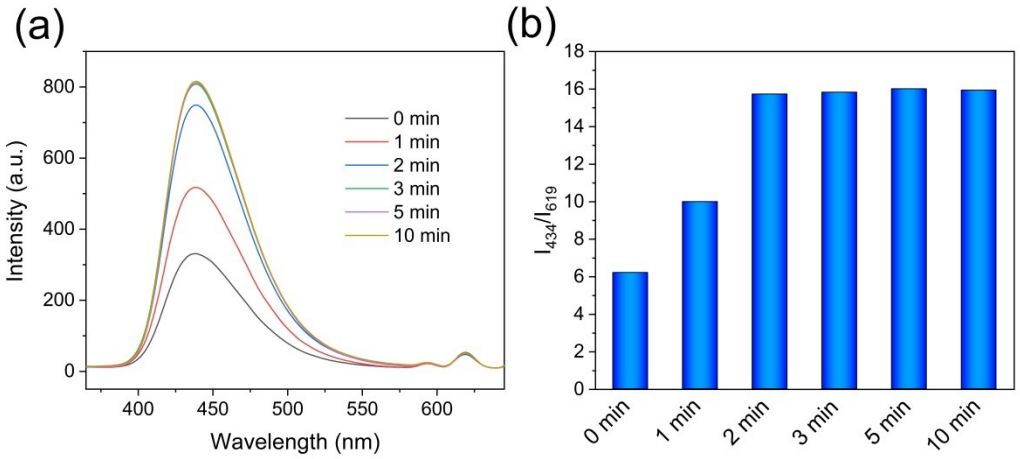

Fig. S5. (a) Fluorescence spectra of Eu-MOF towards DPA at different response time. (b) The fluorescence intensity ratio of I_{434}/I_{621}.

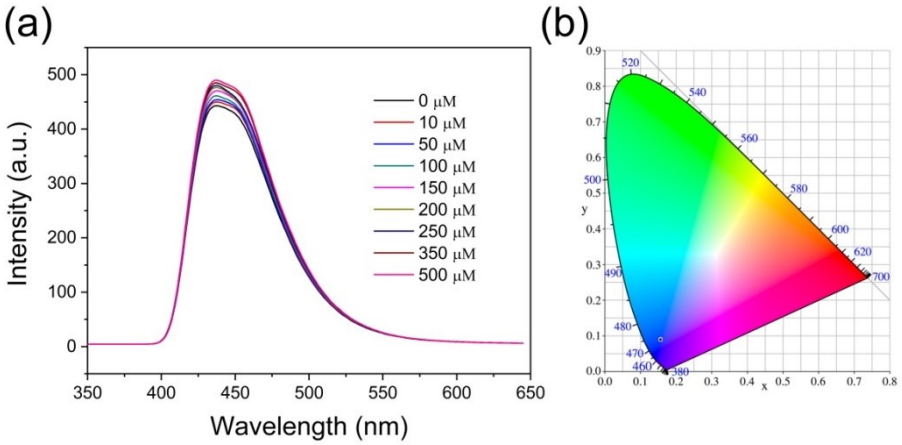

Fig. S6. (a) Fluorescence emission spectra of NH_2-BDC in the presence of different concentrations of DPA. (b) CIE chromaticity diagram of NH_2-BDC in the presence of different concentrations of DPA.

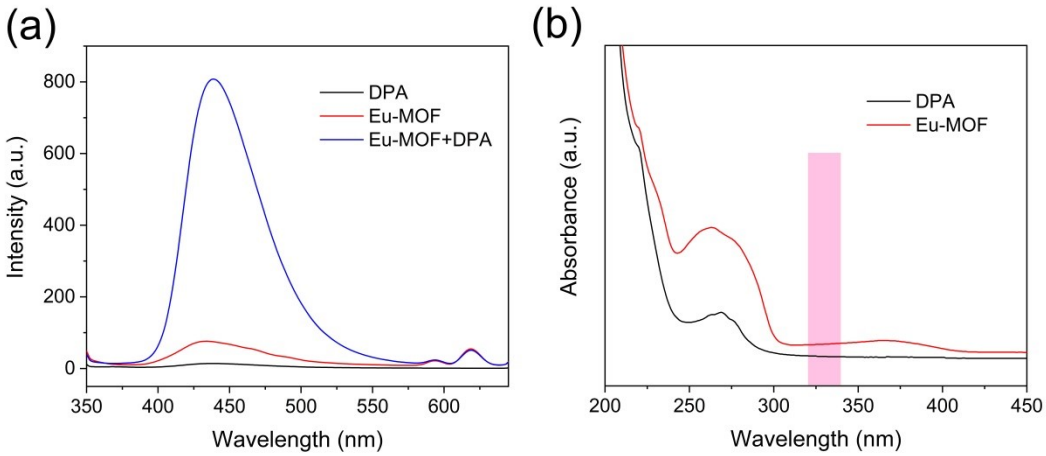

Fig. S7. (a) Fluorescence emission spectra of DPA, Eu-MOF and DPA@Eu-MOF @Eu-MOF. (b) Absorption spectra of DPA and Eu-MOF.

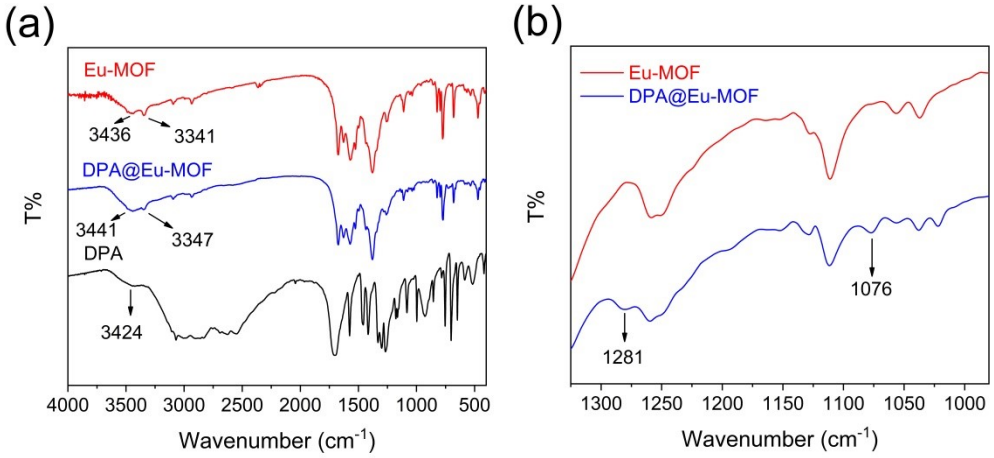

Fig. S8. The FT-IR spectra of Eu-MOF, DPA@Eu-MOF and DPA.

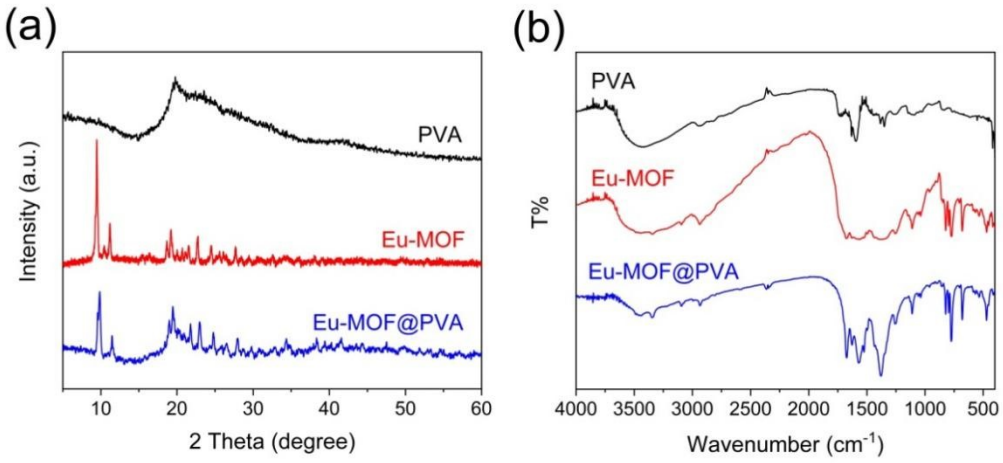

Fig. S9. (a) The PXRD patterns of PVA, Eu-MOF@PVA and Eu-MOF. (b) The FT-IR spectra of PVA, Eu-MOF@PVA and Eu-MOF.

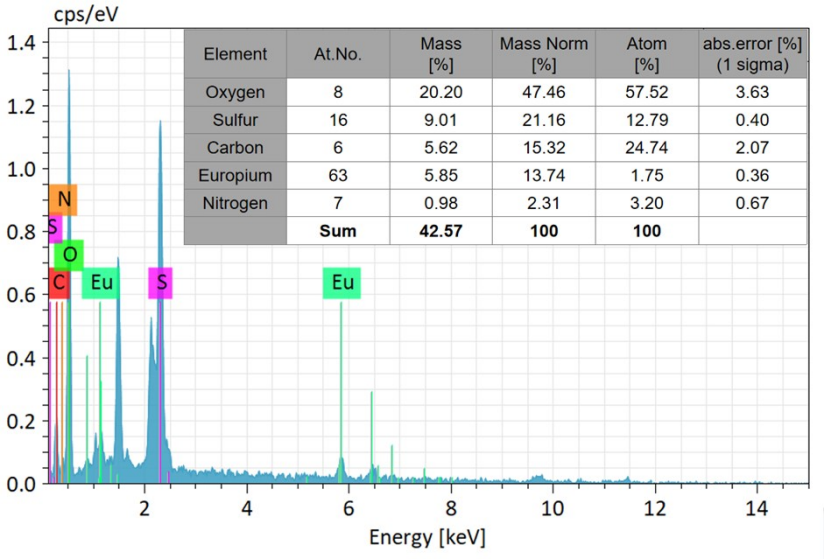

Element	At.No.	Mass [%]	Mass Norm [%]	Atom [%]	abs.error [%] (1 sigma)
Oxygen	8	20.20	47.46	57.52	3.63
Sulfur	16	9.01	21.16	12.79	0.40
Carbon	6	5.62	15.32	24.74	2.07
Europium	63	5.85	13.74	1.75	0.36
Nitrogen	7	0.98	2.31	3.20	0.67
	Sum	**42.57**	**100**	**100**	

Fig. S10. The EDS analyses of Eu-MOF@PVA.

Table S1.Crystal data and structure refinement for Eu-MOF

Empirical formula	$C_{26}H_{18}Eu_2N_3O_{14}S_2$
Formula weight	964.47
Temperature/K	170.0
Crystal system	monoclinic
Space group	C2/c
a/Å	17.4178(12)
b/Å	11.3069(8)
c/Å	18.6828(12)
α/°	90
β/°	117.121(3)
γ/°	90
Volume/Å^3	3274.8(4)
Z	4
ρcalcg/cm^3	1.956
μ/mm^{-1}	21.558
F(000)	1860.0
Crystal size/mm^3	0.06×0.04×0.03
Radiation	GaKα(λ=1.34139)
2Θ range for data collection/°	8.42 to 121.728
Index ranges	-22≤h≤22,-14≤k≤14,-21≤l≤24
Reflections collected	20670
Independent reflections	3773[R_{int} =0.0609,R_{sigma} =0.0450]
Data/restraints/parameters	3773/0/231
Goodness-of-fitonF^2	1.111

Final Rind exes[I>=2σ(I)]	R_1 =0.0416,wR_2 =0.1031
Final Rind exes[alldata]	R_1 =0.0458,wR_2 =0.1052
Largest diff.peak/hole/eÅ^{-3}	2.27/-1.10

Table S2. Bond lengths for Eu-MOF

Atom	Atom	Length/Å
Eu1	Eu1#1	3.9061(5)
Eu1	O1#2	2.324(4)
Eu1	O2#3	2.562(4)
Eu1	O2#4	2.426(4)
Eu1	O3	2.396(4)
Eu1	O4	2.321(4)
Eu1	O5#5	2.384(4)
Eu1	O6	2.356(4)
Eu1	O7#3	2.475(4)
Eu1	C6#3	2.876(5)
S1	C5	1.716(5)
S1	C8	1.720(5)
O1	C3	1.258(6)
O2	C6	1.279(6)
O3	C11	1.250(7)
O4	C3	1.249(6)
O5	C7	1.252(5)
O6	C1	1.258(5)
O7	C6	1.245(6)
C1	C2	1.483(10)
N1	C11	1.312(7)
N1	C14	1.450(10)
N1	C15	1.459(10)
C2	C10	1.406(7)
C2	C10#1	1.406(7)
C3	C5	1.480(7)
C4	C8	1.367(8)
C4	C9	1.407(7)
C5	C9	1.354(7)
C6	C8	1.471(7)
C7	C12	1.469(10)
C10	C13	1.320(11)
C10	N3	1.27(3)

Atom	Atom	Length/Å
C12	C13#1	1.421(7)
C12	C13	1.421(7)
C13	N2	1.370(19)

#**1**:1-X,+Y,1/2-Z; #**2**:1-X,-Y,1-Z; #**3**:1/2-X,-1/2+Y,1/2-Z; #**4**:1/2+X,-1/2+Y,+Z; #**5:**+X,-1+Y,+Z

Table S3. Bond lengths [Å] and angles [°] for Eu-MOF

Atom	Atom	Atom	Angle/°
O1#1	Eu1	Eu1#2	142.32(9)
O1#1	Eu1	O2#3	122.10(12)
O1#1	Eu1	O2#4	135.18(12)
O1#1	Eu1	O3	75.57(14)
O1#1	Eu1	O5#5	73.79(13)
O1#1	Eu1	O6	146.87(13)
O1#1	Eu1	O7#4	87.96(14)
O1#1	Eu1	C6#4	110.58(14)
O2#3	Eu1	Eu1#2	39.71(9)
O2#4	Eu1	Eu1#2	37.23(8)
O2#3	Eu1	O2#4	76.94(13)
O2#3	Eu1	O7#4	122.98(12)
O2#3	Eu1	C6#4	99.48(13)
O2#4	Eu1	C6#4	26.41(13)
O3	Eu1	Eu1#2	118.21(10)
O3	Eu1	O2#3	81.53(13)
O3	Eu1	O2#4	148.92(13)
O3	Eu1	O7#4	155.42(13)
O3	Eu1	C6#4	171.34(15)
O4	Eu1	Eu1#2	131.00(9)
O4	Eu1	O1#1	83.18(13)
O4	Eu1	O2#3	145.31(14)
O4	Eu1	O2#4	102.48(13)
O4	Eu1	O3	82.93(14)
O4	Eu1	O5#5	142.80(15)
O4	Eu1	O6	73.83(14)
O4	Eu1	O7#4	77.00(15)
O4	Eu1	C6#4	91.64(14)
O5#5	Eu1	Eu1#2	68.83(9)
O5#5	Eu1	O2#3	71.47(13)
O5#5	Eu1	O2#4	76.08(13)
O5#5	Eu1	O3	117.72(15)

Atom	Atom	Atom	Angle/°
O5#5	Eu1	O7#4	73.42(16)
O5#5	Eu1	C6#4	70.51(15)
O6	Eu1	Eu1#2	69.10(9)
O6	Eu1	O2#4	74.23(12)
O6	Eu1	O2#3	72.71(13)
O6	Eu1	O3	78.15(14)
O6	Eu1	O5#5	137.51(14)
O6	Eu1	O7#4	109.12(15)
O6	Eu1	C6#4	93.89(14)
O7#4	Eu1	Eu1#2	85.95(9)
O7#4	Eu1	O2#4	51.71(12)
O7#4	Eu1	C6#4	25.52(13)
C6#4	Eu1	Eu1#2	60.88(10)
C5	S1	C8	91.3(3)
C3	O1	Eu1#1	138.4(4)
Eu1#6	O2	Eu1#7	103.06(13)
C6	O2	Eu1#6	144.8(3)
C6	O2	Eu1#7	90.6(3)
C11	O3	Eu1	130.5(4)
C3	O4	Eu1	154.8(4)
C7	O5	Eu1#8	137.9(4)
C1	O6	Eu1	138.4(4)
C6	O7	Eu1#7	95.5(3)
O6	C1	O6#2	124.6(7)
O6	C1	C2	117.7(3)
O6#2	C1	C2	117.7(3)
C11	N1	C14	121.4(6)
C11	N1	C15	120.3(7)
C14	N1	C15	118.1(1)
C10#2	C2	C1	120.9(4)
C10#2	C2	C10	118.1(8)
O1	C3	C5	117.4(4)
O4	C3	O1	126.4(5)
O4	C3	C5	116.2(4)
C8	C4	C9	112.4(5)
C3	C5	S1	119.8(4)
C9	C5	S1	111.8(4)
C9	C5	C3	128.4(5)
O2	C6	Eu1#7	63.0(3)

Atom	Atom	Atom	Angle/°
O2	C6	C8	119.6(4)
O7	C6	Eu1#7	59.0(3)
O7	C6	O2	121.1(5)
O7	C6	C8	119.2(4)
C8	C6	Eu1#7	168.5(4)
O5#2	C7	O5	124.0(7)
O5#2	C7	C12	118.0(4)
O5	C7	C12	118.0(4)
C4	C8	S1	111.5(4)
C4	C8	C6	129.4(5)
C6	C8	S1	119.2(4)
C5	C9	C4	113.0(5)
C13	C10	C2	121.7(7)
N3	C10	C2	121.9(15)
N3	C10	C13	116.2(14)
O3	C11	N1	123.8(6)
C13#2	C12	C7	120.6(4)
C13	C12	C7	120.6(4)
C13#2	C12	C13	118.9(8)
C10	C13	C12	119.8(7)
C10	C13	N2	115.7(9)
N2	C13	C12	124.4(9)

#**1**:1-X,-Y,1-Z; #**2**:1-X,+Y,1/2-Z; #**3**:1/2+X,-1/2+Y,+Z; #**4**:1/2-X,-1/2+Y,1/2-Z; #**5**:+X,-1+Y,+Z; #**6**:-1/2+X,1/2+Y,+Z; #**7**:1/2-X,1/2+Y,1/2-Z; #**8**:+X,1+Y,+Z

Table S4. The comparison of different MOFs for DPA detection

Probe	LOD (μM)	Linear range (μM)	Ratiometric response	Ref.
$Tb_{0.9}Gd_{0.1}$-PBA	1.03	0-210	Dual	[5]
Er-BTC-MOF/MIP-r-QCNS	1.28	10-125	Single	[6]
Fe-MIL-88NH_2	1.46	10-60	Single	[7]
Ca_3(ddpa) $\cdot 7H_2O$	1.01	0-120	Single	[8]
$Tb_4L_6(DMF)_5(H_2O)_3]\cdot 5DMF \cdot 6H_2O$	1.7	0-50	Single	[9]
$Tb_{0.533}Eu_{0.467}$-$(Hcppa)_{1.5}(H_2O)(DMF)]\cdot 3H_2O$	2.29	0-850	Dual	[10]
Eu-MOF	0.41	0-500	Dual	This work

Notes and references

[1] G. Kresse, J. Furthmüller, Efficiency of ab-initio total energy calculations for metals and

semiconductors using a plane-wave basis set, *Comput. Mater. Sci*, 6 (1996) 15-50.

[2] J.P. Perdew, K. Burke, M. Ernzerhof, Generalized Gradient Approximation Made Simple, *Phys. Rev. Lett.*, 77 (1996) 3865-3868.

[3] P.E. Blochl, Projector augmented-wave method, *Phys Rev B Condens Matter*, 50 (1994) 17953-17979.

[4] S. Grimme, Semiempirical GGA-type density functional constructed with a long-range dispersion correction, *J Comput Chem*, 27 (2006) 1787-1799.

[5] Y. Songlin, S. Dongxue, L. Kaisu, W. Lei, Z. Ying, S. Yaguang, Z. Mingchang, W. Shuangyan, Synthesis of a lanthanide-based bimetallic-metal-organic framework for luminescence sensing anthrax biomarker, *Dyes Pigm.*, 220 (2023) 111673.

[6] S. Norouzi, K. Dashtian, F. Amourizi, R. Z. Dorabei, Red-emissive carbon nanostructure-anchored molecularly imprinted Er-BTC MOF: a biosensor for visual anthrax monitoring, *Analyst,* 148 (2023) 3379-3391.

[7] D. Deng, J. Xu, T. Li, D. Tan, Y. Ji, R. Li, Dual-mode strategy for 2,6-dipicolinic acid detection based on the fluorescence property and peroxidase-like activity inhibition of Fe-MIL-88NH_2, Spectrochim. *Acta, Part A*, 291 (2023) 122363.

[8] Z. Cong, M. Zhu, Y. Zhang, W. Yao, M. Kosinova, V.P. Fedin, S. Wu, E. Gao, Three novel metal-organic frameworks with different coordination modes for trace detection of anthrax biomarkers, *Dalton Trans.*, 51 (2022) 250-256.

[9] P. P. Zhang, A. Y. Ni, J. J. Zhang, B. L. Zhang, H.A. Zhou, H. Zhao, S. Liu, J. Ni, C. Duan, Tb-MOF-based luminescent recovery probe for rapid and facile detection of an anthrax biomarker, *Sens. Actuators, B*, 384 (2023) 133624.

[10] Q. Wang, J. Dong, Z. Li, X. Wang, Y. He, B. Chen and D. Zhao, Dual-emitting mixed-lanthanide metal-organic framework for ratiometric and quantitative visual detection of 2,6-Pyridine Dicarboxylic Acid, *Inorg. Chem.*, 2023, 62, 14439-14447.